JOURNAL OF CATALYSIS **172,** 55–63 (1997)
ARTICLE NO. CA971865

Ammoxidation of Propane on Nickel Antimonates

The Role of Vanadium as Promoter

T. J. Cassidy, M. Pollastri, and F. Trifirò[1]

Dipartimento di Chimica Industriale e dei Materiali, Viale Risorgimento 4, 40136 Bologna, Italy

Received January 2, 1997; revised June 23, 1997; accepted July 28, 1997

The catalytic behaviour of Ni–Sb mixed oxides doped by vanadium has been investigated for the ammoxidation of propane and propene to acrylonitrile. The binary nickel antimonates, with 1 : 1 < Ni : Sb < 1 : 3, were found to be active and selective in the ammoxidation of propene to acrylonitrile (selectivity >80%) but they showed no activity in propane ammoxidation till 470°C. The activity/gram and the yield in acrylonitrile (ACN)/gram presented a maximum at Ni : Sb 1 : 2 due to a balance between the surface area and the doping effect of antimony. With the addition of vanadium to the Ni–Sb system, the activity and productivity of the catalysts were increased markedly, both in propane and propene ammoxidation. The optimum vanadium loading in terms of ACN yield was found for $NiSb_2O_6$ to be V : Ni 0.2 : 1 atomic ratio, a compromise between activity and selectivity. It was found that sites containing vanadium are involved in the selective nitrogen insertion step in propene ammoxidation, as well as in the activation of propane. The ammoxidation of propane is a cleaner reaction than the ammoxidation of propene, as smaller amounts of hydrogen cyanide (HCN) and acetonitrile (AceN) were formed for the same yield of acrylonitrile. X-ray analysis revealed the presence of $NiSb_2O_6$ and free αSb_2O_4 in all samples. In the Ni–Sb vanadium doped oxides the FTIR characterisation showed that up to a V : Ni ratio of 0.2, vanadium species different from V_2O_5, and very likely interacting with the $NiSb_2O_6$, were formed; these species are the ones involved in propane activation. With higher loadings of vanadium, V_2O_5 species formed which are responsible for the lowering of acrylonitrile selectivity. © 1997 Academic Press

1. INTRODUCTION

Acrylonitrile is a key raw material in the production of acrylic fibres for clothing and high-performance thermoplastics such as ABS (acrylonitrile-butadiene-styrene) and SAN (styrene-acrylonitrile) resins. It is a large-scale process and it is predicted that the worldwide demand for acrylonitrile in the year 2000 will be over five million tons. Today, over 90% of acrylonitrile is produced by propene ammoxidation but there has been growing interest during the past decade in developing a cheaper alternative. The activation of alkanes is gradually becoming an achievable industrial goal. However, the conversion of *n*-butane to maleic anhydride (1) is presently the only large-scale process which uses a paraffin as the primary hydrocarbon reactant. In many cases the use of the alkane, as opposed to the alkene, is desirable from an economic viewpoint because their market value is lower. Pilot plants already exist for propane ammoxidation (2) and there is a considerable amount of patent literature concerning possible catalytic formulations; see, for example (3–7):

$$CH_3{-}CH_2{-}CH_3 + NH_3 + 2O_2 \Rightarrow CH_2{=}CH{-}CN + 4H_2O \quad (\Delta H = -632\,\text{kJ/mol}).$$

Several groups have recently published results in the open literature on the role of different catalytic systems, including $GaSbO_x$ (8), $BiVMoO_x$ (9, 10), and $SbVO_x$ (11–16), $MoVNbTeO_x$ (17); $SnVSbO_x$, as well as on mechanistic aspects of the reaction (18). The best catalytic performance was achieved using a $V : Sb : WO_x$ 1 : 5 : 1, producing yields in acrylonitrile between 35–40% (12). The vanadium antimonate, having a rutile crystalline structure, is known as a paraffin activator (12).

In this paper the catalytic behaviour in the ammoxidation of propane and propene of pure $NiSb_2O_6$, and doped with vanadium, was investigated. $NiSb_2O_6$ has a trirutile structure (19) (two neighbouring antimony atoms are present), similar to the rutile structure of $SbVO_4$, the most investigated catalyst for propane ammoxidation. The aim of this work was to stabilise vanadium species in a rutile structure similar to $VSbO_4$, but with different neighbours, which may contribute to the reaction mechanism increasing activity and selectivity in acrylonitrile production.

2. EXPERIMENTAL

2.1. Stoichiometric and Nonstoichiometric Binary Nickel Antimonates

A series of nickel antimonates with the following atomic ratios Ni : Sb 1 : 1, Ni : Sb 1 : 2 (stoichiometric ratio), and

[1] Corresponding author.

0021-9517/97 $25.00

TABLE 1

Calcination Temperature and Surface Areas of the Binary and Ternary Catalysts

Catalyst (atomic ratio)	Calcination temp. (°C)	Surface area (m^2/g)
NiSb 1/1	700	14
NiSb 1/2	700	40
NiSb 1/3	700	38
NiSbV 1/2/0.1	700	56
NiSbV 1/2/0.2	700	44
NiSbV 1/2/0.3	700	28
NiSbV 1/2/0.2	300	102
NiSbV 1/2/0.2	500	86
NiSbV 1/2/0.2	800	8

Ni : Sb 1 : 3 were prepared as follows. Nickel chloride and antimony pentachloride were dissolved in an aqueous HCl solution. The resulting green solution was added dropwise into a vigorously stirred ammonium acetate buffer solution (pH 7), upon which the metal salts coprecipitated. During the coprecipitation the pH was maintained at 7 by the dropwise addition of concentrated NH_3 solution. The resulting pale grey/green precipitate was washed thoroughly with distilled water three times and centrifuged after each wash. The catalyst precursor was dried overnight at 120°C, the temperature was then raised slowly to 300°C held for 2 h, before being raised to 700°C. The catalyst precursor was left overnight (16 h) at this temperature to yield the active catalyst. All catalysts were pressed and sieved (30–40 mesh) before catalytic testing. Table 1 lists the surface areas of the catalysts.

2.2. Vanadium-Doped Ternary Nickel Antimonates

A second series of nickel antimonates was doped with increasing vanadium loadings, from 0 to 0.3 V/Ni atomic ratio (atomic ratio being the V : Ni ratio). The preparation procedure was identical to that described above (Section 2.1) with the exception that vanadyl acetylacetonate was dissolved in the correct mole ratio during the initial step when the salts were dissolved in HCl(aq). An excess of the ternary catalyst (Ni : V : Sb 1 : 0.2 : 2) was prepared for studying the effect of the calcination temperature on the physical characterisation of the catalysts. The surface area of the ternary catalysts are listed in Table 1.

2.3. Characterisation

Surface area measurements were determined using the BET method on a Carlo Erba Sorpty 1750 apparatus by N_2 adsorption; 0.5 g of powdered catalyst was used for each sample. FT-IR spectra were recorded using a Perkin Elmer 1750 spectrometer by means of the conventional self-supporting disk technique (0.5% in KBr). Powder XRD data were collected on a Philips PW1050/81 diffractometer, using Cu Kα radiation ($\lambda = 0.15418$ nm).

The catalytic data were collected using a stainless steel, fixed bed, down flow microreactor. The normal feed gas ratios were 10% propane, 10% oxygen, and 5% ammonia and 2.5% propene, 10% oxygen, and 5% ammonia, with helium as the diluent in all cases. All gas flows were individually controlled with Brooks mass flow meters; the operating pressure was atmospheric. Generally, 2 cm^3 of pelleted catalyst was loaded into the reactor and a contact time of 2 s was always used. Plugs of glass wool were used to keep the catalytic bed within the reactor and a thermocouple recorded the bed temperature. Analysis of the heavy products/reactants—propane, propene, acetonitrile (AceN), and acrylonitrile (ACN)—was done by means of a Carlo Erba 6000 vega series 2 FID GC. A six-port valve, situated at the outlet of the reactor, enabled postreactor samples to be eluted onto a Porapak QS column. The light products/reactants—oxygen, nitrogen, CO, and CO_2—were manually extracted from the postreactor gas stream (1 ml via a PTFE septum) and injected into a Carlo Erba 4300 TCD GC fitted with a carbo-sieve column. The ammonia concentration was calculated by adsorption (for 5 min) in an acid solution (15 ml 0.1 *M* HCl) followed by back titration with NaOH 0.1 *M*. Hydrogen cyanide production was also analysed by adsorption (in 15 ml NaOH 0.1 *M*) and back titration (with $AgNO_3$ 0.1 *M*, after the addition of 2 ml KI 1 *M* and 6 ml of NH_3 6 *M*), a procedure known as the Liebig–Dénigès method. Product analysis was performed over a series of temperatures between 190 and 500°C, ranging from 0 to 100% conversion in O_2 over an active catalyst. Four analyses were made at each temperature following a 30-min equilibration period; the average value was recorded.

3. RESULTS AND DISCUSSION

3.1. Surface Area Measurements

The surface area of each catalyst was measured after calcination. The surface areas of the catalysts depended on: (i) the metal ratio, (ii) the addition of vanadium, and (iii) the temperature of calcination. The trends of the three sets of catalysts are clear. The binary nickel antimonate catalyst NiSb 1/1 has a markedly lower surface area than the stoichiometric ($NiSb_2O_6$) and excess antimony containing catalysts. The ternary catalysts show a decrease in surface area as the vanadium content is increased. By increasing the calcination temperature from 300 to 800°C, a drastic decrease in the surface area, from 102 to 8 m^2/g, is observed.

3.2. Powder XRD Studies

Figure 1 shows the XRD patterns of the three catalyst series after calcination and before catalytic testing. The reflections at 27.2, 35.1, and 53.3 2θ are the three primary

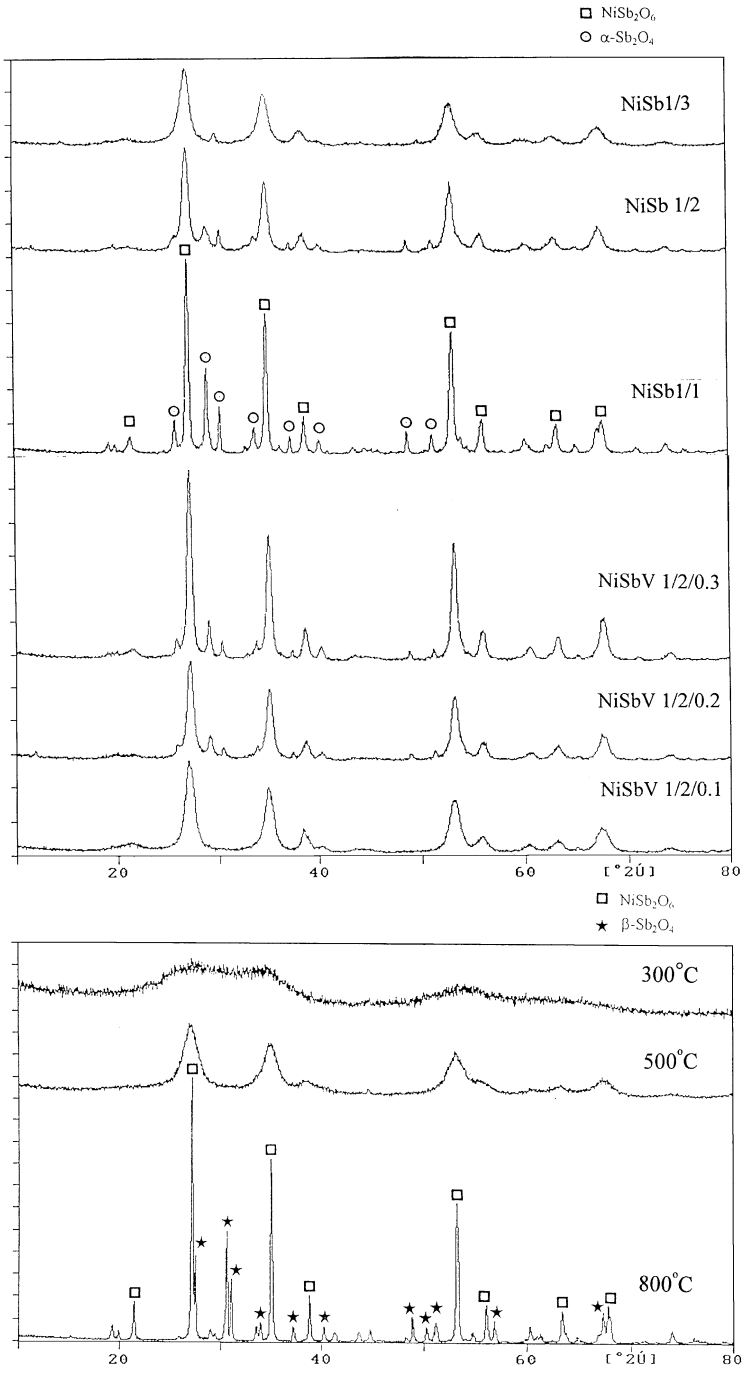

FIG. 1. Powder XRD patterns of the binary nickel antimonates, NiSb 1/1, NiSb 1/2, NiSb 1/3; the ternary nickel antimonates, NiSbV 1/2/0.1, NiSbV 1/2/0.2, NiSbV 1/2/0.3; and ternary sample NiSbV 1/2/0.2 calcinated at various temperatures, NiSbV 1/2/0.2, $T = 300$; NiSbV 1/2/0.2, $T = 500$; and NiSbV 1/2/0.2, $T = 700$.

reflections of the $NiSb_2O_6$ tri-rutile structure (20, 24, 25). The diffraction patterns of NiSb 1/2 and NiSb 1/3 are relatively broad, indicating the formation of small crystallites in agreement with the higher surface area. NiSb 1/1, on the other hand, has a more defined pattern. In the spectra of NiSb 1/1 and 1/2, the reflections due to α-Sb_2O_4 can be seen at 29.0, 30.4, and 33.8 2θ, although always in small amounts. Evidence of trace amounts of Sb_6O_{13} can be seen in NiSb 1/3 (the reflection at 30.0 is clearly visible).

Upon the addition of vanadium to the nickel antimonate system, the XRD reflections show no change in position (Fig. 1). Only an increase of crystallinity is observed ($SbVO_4$

reflections are very similar to those of $NiSb_2O_6$ and would be difficult to identify if present in small amounts).

In Fig. 1 the evolution of the crystallites is followed as a function of calcination temperature. It can be seen that, even at 300°C, the characteristic tri-rutile reflections are present, albeit very weak and diffuse, indicating that the microcrystalline structure forms during preparation. As the temperature of calcination is raised to 500°C the reflections become more clearly defined and the minor nickel antimonate peaks appear. Figure 1 shows that the evolution of the α-Sb_2O_4 phase appears at 700°C. The catalyst calcined at 800°C no longer has the reflections due to α-Sb_2O_4, but rather it has the characteristics of β-Sb_2O_4, indicating the phase transition of the free antimony oxide at this temperature, in agreement with the literature (21).

3.3. FT-IR Studies

Figure 2 shows the FT-IR spectra of the binary nickel antimonate $NiSb_2O_6$, of α-Sb_2O_4, of vanadium-doped α-Sb_2O_4 (V : Sb 0.2 : 1) and of the ternary nickel antimonates with increasing vanadium loadings. All spectra were measured after calcination and before catalytic testing. In all spectra the bands of α-Sb_2O_4, as well as those of $NiSb_2O_6$, are detected. The bands at ~710, 635, 600, 535, and 512 cm^{-1} are attributed to $NiSb_2O_6$ (22). It should be noted that it is difficult to differentiate α-Sb_2O_4 and the $NiSb_2O_6$ from their IR spectra, and that NiO has no IR active bands in the investigated region.

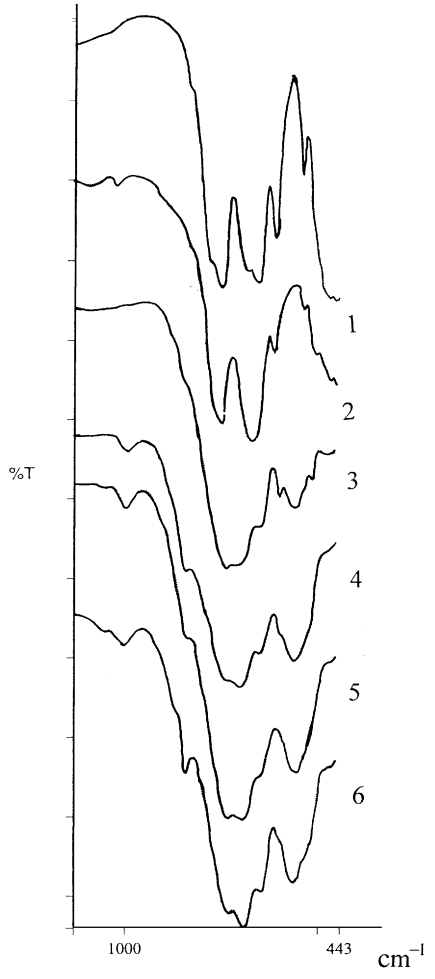

FIG. 2. FT-IR spectra of: 1, αSb_2O_4; 2, vanadium doped αSb_2O_4 (V : Sb = 0.2); 3, $NiSb_2O_6$; 4, NiSbV 1/2/0.1; 5, NiSbV 1/2/0.2.2; and 6, NiSbV 1/2/0.3.

With the addition of vanadium, some new bands appear: a band at ~995 and 840 cm^{-1}, and in sample NiSbV 1/2/0.3, also a band at 1020 cm^{-1}.

The band at 1020 cm^{-1} can be attributed to the V=O group of free V_2O_5. In order to interpret the other new bands, it is useful to compare with the spectra of α-Sb_2O_4 doped with vanadium (V : Sb 0.2 : 1). A band present at 1016 cm^{-1} is visible, very close to the 1020 cm^{-1} band of pure V_2O_5. Therefore we attribute the new bands appearing in the vanadium-doped nickel antimonate sample to vanadium species interacting with the $NiSb_2O_6$ rutile. The band at 995 cm^{-1} is characteristic of a weakened V=O stretch (23). The band at ~840 cm^{-1} can be attributed to a V–O–Sb bending mode (V–O–V is at 823 cm^{-1}).

The postreaction spectra showed no changes in all catalysts, apart from NiSbV 1/2/0.3, where the band associated with free V_2O_5 had strongly decreased.

3.4. Microreactor Tests

As a blank test run, the normal feed gases were passed through the empty reactor and the exit gases analysed. Negligible conversion of propane occurred in the temperature range used in the catalytic runs, that is between 200 and 500°C. Likewise, the homogeneous oxidation of ammonia to dinitrogen and water reached a maximum of only 3% at 480°C.

3.4.1. The binary system. The three binary catalysts showed poor activity in the ammoxidation of propane; they showed appreciable activity only at temperatures above 470°C. For this reason, propene rather than propane was used as the hydrocarbon feed with the binary catalysts. The actual yields in the several products of the three catalysts at 390°C are plotted in Fig. 3. Figure 4 shows the selectivity of the three binary catalysts at 20% conversion in the ammoxidation of propene. The values of conversion per unit surface area at $T = 460$°C for the three catalysts are (Fig. 5), in declining order, NiSb 1/1 = 3.63% gm^{-2}, NiSb 1/2 = 2.35% gm^{-2}, and NiSb 1/3 = 0.87% gm^{-2}. Therefore the specific activity decreases with the increase in the amount of antimony oxides, however, the activity per gram maximises for the sample NiSb 1/2 owing to an increase in surface area. All three catalysts demonstrate remarkable selectivity; CO_x production was negligible and is, therefore, not included in the diagram. As the antimony ratio increases, there is a very slight increase in selectivity

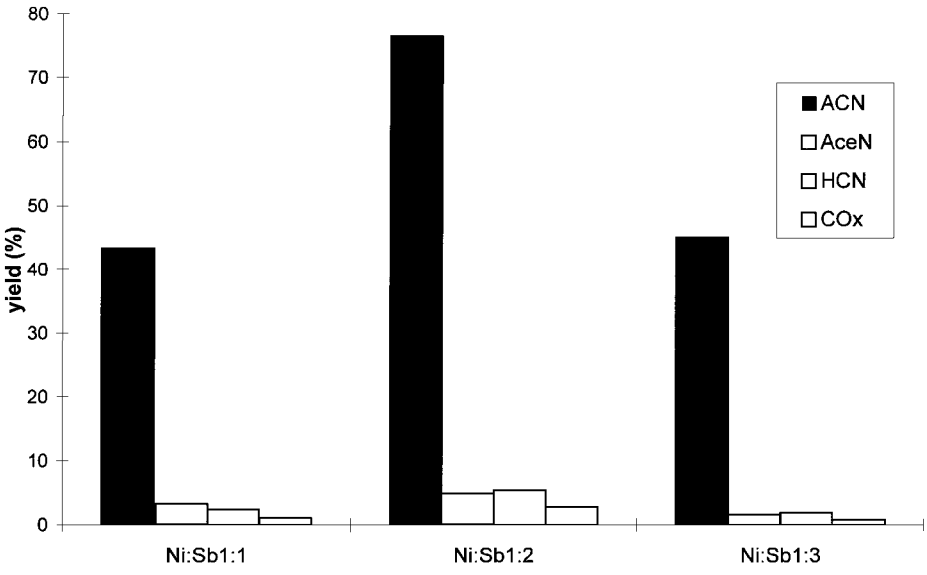

FIG. 3. Yields of products over the binary catalysts in the ammoxidation of propene. Reaction conditions: $C_3 = 2.5\%$; NH_3 5%; O_2 10%; $T = 460°C$; $\tau = 2$ s.

to acrylonitrile, together with a decrease in selectivity to acetonitrile and hydrogen cyanide. The nickel antimonate NiSb 1/2 produces the highest yield of acrylonitrile per gram of catalyst. For this reason it was chosen as the basic antimonate for further studies of the effect of vanadium addition.

3.4.2. The ternary system. As mentioned above, the pure nickel antimonate NiSb 1/2 is not active in propane conversion at temperatures below 470°C. With increasing amounts of vanadium, the activity is markedly improved. Figure 6 shows the conversion of propane/surface area at isothermal conditions (390°C). As the vanadium loading increases to 0.2 atomic ratio, the catalytic activity of catalyst improves linearly, and then increases more rapidly. Figure 7 compares the yield in ACN, AceN, and CO_x at 20% propane conversion, with respect to the vanadium loading. In the same figure we have reported the temperature at which 20% of conversion was reached. A loading of 0.2 atomic ratio vanadium leads to the best compromise between ACN yield and CO_x production. The catalyst containing 0.3 atomic ratio of vanadium is less selective to ACN because deep oxidation products are favoured. NiSbV 1/2/0.1 showed good selectivity but required higher temperatures to obtain

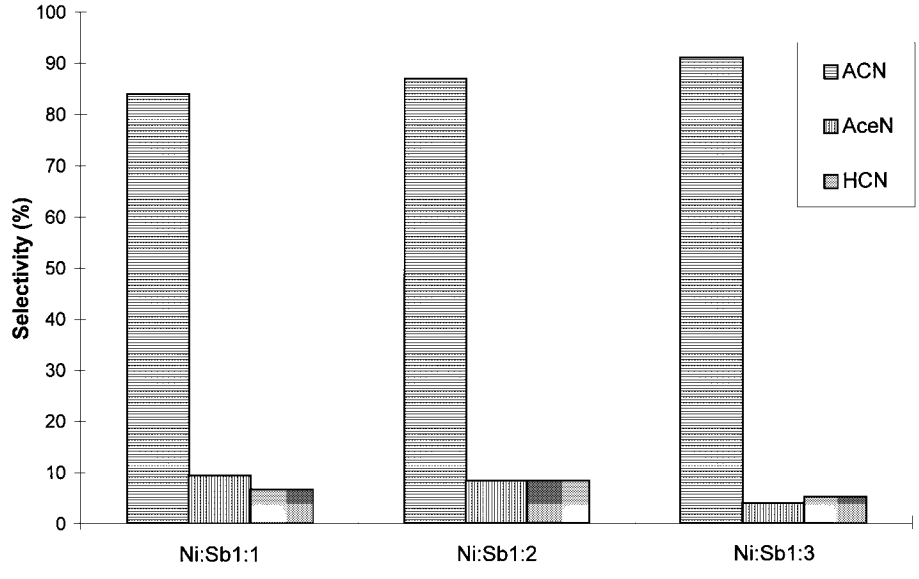

FIG. 4. Selectivity to ACN, AceN, and HCN in the ammoxidation of propene over the binary catalysts at 20% C_3 = conversion.

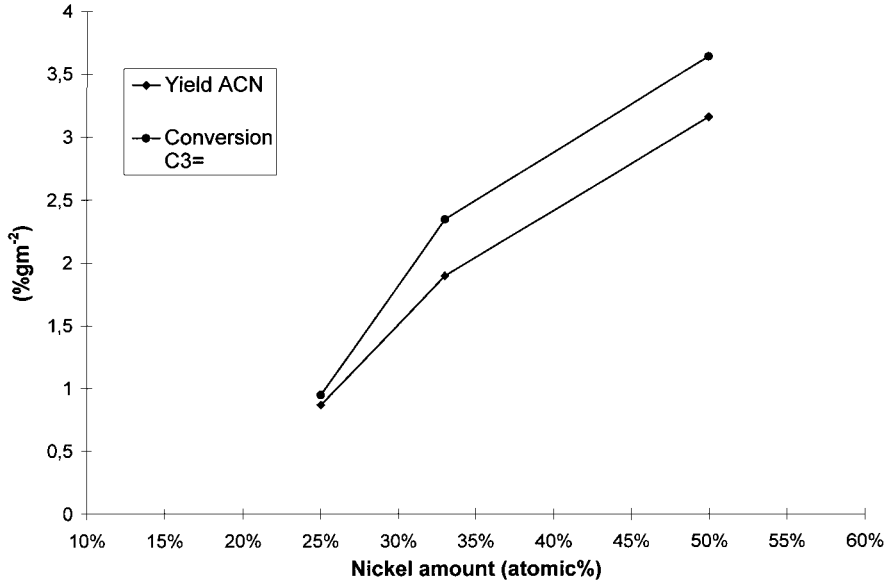

FIG. 5. Conversion of propene/surface area and yield in ACN/surface area as a function of nickel content reaction conditions: $C_3 = 2.5\%$; NH_3 5%; O_2 10%; $T = 390°C$; $\tau = 2$ s.

the desired conversion. Figure 8 shows the distribution of products over the temperature range between 390 and 462°C, obtained on catalyst NiSbV 1/2/0.2. The selectivity to ACN increases to a maximum between 50 and 55% at ∼450°C, above which the total oxidation products, predominantly CO_2, become significant. The trend in ACN yield does not reach a maximum but continues to rise, indicating that, once produced, ACN is not converted to other products in consecutive reactions. The selectivity to propene and HCN is slightly higher at lower temperatures ∼390°C than at higher ones, indicating an increase in the rate of ACN production from propene as the temperature increases. The addition of vanadium increases the activity, while maintaining a good selectivity to ACN, above 0.2 atomic ratio of vanadium CO_x production becomes significant (see Fig. 7), this occurs concurrently with the appearance of V_2O_5 in the IR spectra.

To investigate the effect of vanadium on the mechanism of the ammoxidation reaction, tests were carried out using propene as the feed gas using the ternary catalysts. The feed gas ratios were 2.5% propene, 5% ammonia, and 10% oxygen. For comparison we report in Table 2 the data of Sb : V 1 : 0.2 prepared with the same method of NiSb based system. The experimental conditions were: $T = 390°C$; $\tau =$ 2 s, and catalyst weight = 2 g.

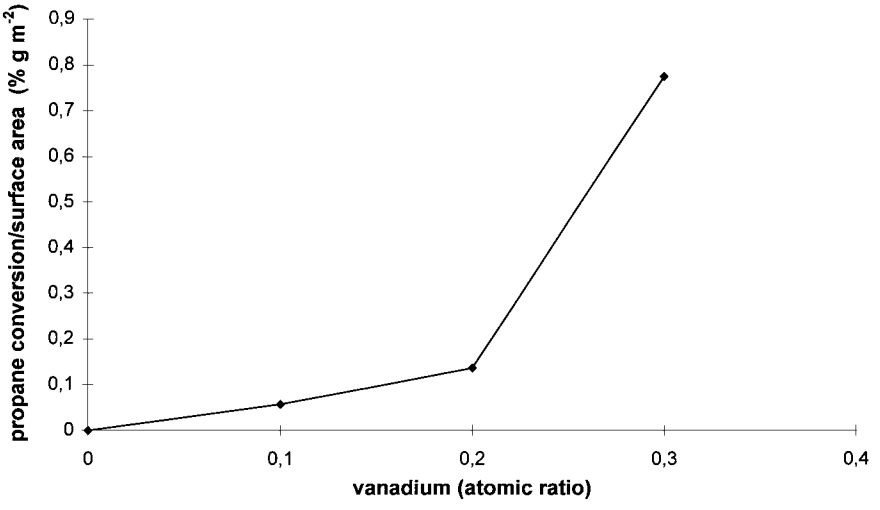

FIG. 6. Conversion of propane/surface area as a function of vanadium content. Reaction conditions: C_3 10%; NH_3 5%; O_2 10%; $T = 390°C$; $\tau = 2$ s.

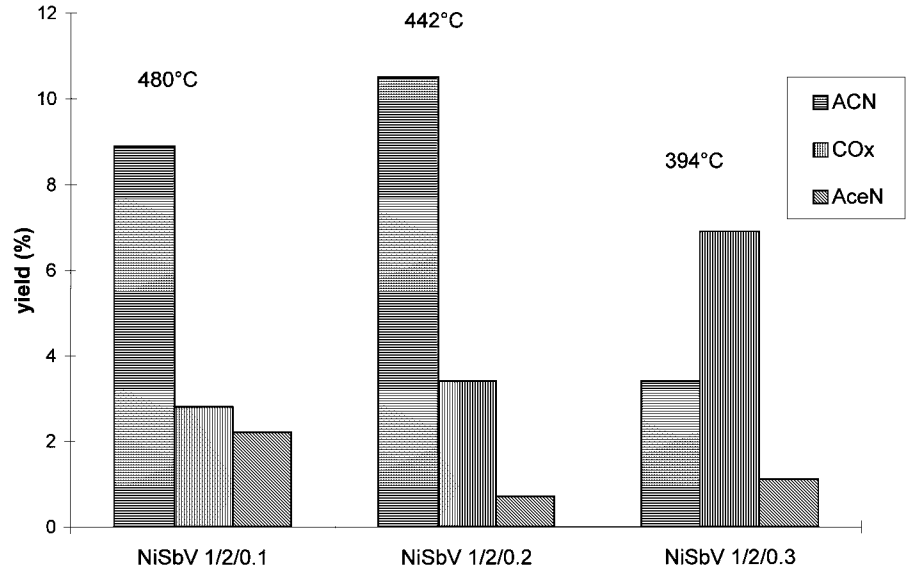

FIG. 7. Yields of ACN, AceN, and HCN, at 20% propane conversion, over the ternary catalysts. Reaction conditions: C_3 10%; NH_3 5%; O_2 10%; T = reported in figure; $\tau = 2$ s.

4. GENERAL DISCUSSION AND CONCLUSIONS

4.1. The Key Properties of Ni–Sb Mixed Oxide

The Ni–Sb mixed oxides were inactive in propane ammoxidation at temperatures below 470°C, but showed good activity in propene ammoxidation. With propene as the feed hydrocarbon, the selectivities to ACN are all high (85–95% at 20% conversion, Fig. 4), rising slightly as the antimony content increases. The activity per gram presented a maximum for NiSb 1/2 (Fig. 3). The surface area increases with the addition of antimony up to the stoichiometric ratio of Sb : Ni (2 : 1), after which it remains essentially constant. The most active catalyst in terms of yield in ACN per unit surface area was the NiSb 1/1 catalyst (Fig. 5). The yield per unit area decreases strongly with increasing antimony content. This in turn implies that the antimony atoms, in excess of a 1 : 2 ratio, dilute the active sites and, in doing so, increase the selectivity to ACN slightly (also known as site isolation (26)). The poor yield per gram of catalyst, obtained with NiSb 1/1, is due to its low surface area, whereas with NiSb 1/3, the decrease in yield with respect to NiSb 1/2 is due to the increase in antimony, resulting in a poisoning

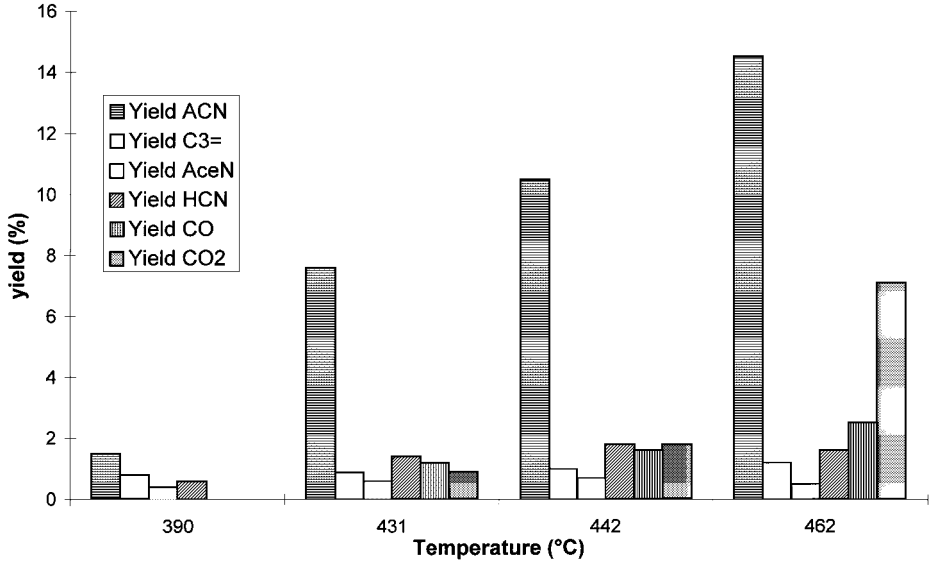

FIG. 8. Distribution of products over catalyst NiSbV 1/2/0.2 as a function of temperature. Reaction conditions: C_3 10%; NH_3 5%; O_2 10%; $\tau = 2$ s.

TABLE 2

A Comparison of Catalytic Data for Three Different Catalytic Systems in the Ammoxidation of Propene

Catalyst	Atomic ratio	Conversion of $C_3^=$ (%)	Selectivity to ACN (%)	Yield in ACN (%)
NiSb	1:2	20	87	17.4
NiVSb	1:0.2:2	98	76	74.5
SbV	1:0.2	55	51	28

effect (the surface area remains essentially equal). The higher yield in ACN per gram of catalyst with NiSb 1/2 is due to the compromise between catalytic activity and selectivity to ACN. The fact that the selectivity of all three catalysts at equal conversion remains practically the same must be in favour of the hypothesis that excess antimony ions play essentially the role of diluting the active sites.

From XRD and FTIR analysis the major phase in all three binary catalysts is the tri-rutile, $NiSb_2O_6$. No evidence for NiO was found, which is especially surprising for the NiSb 1/1 catalyst.

4.2. The Role of Vanadium

With the addition of vanadium to $NiSb_2O_6$, not only the activity in propene ammoxidation increases, but the catalysts also become active in the ammoxidation of propane. At the same time, the selectivity to ACN is reduced due to an increase in total combustion products. The best compromise in terms of ACN yield was NiSbV 1/2/0.2. New FT-IR bands appear which are assigned to a vanadium species interacting with the bulk tri-rutile structure. Propane conversion rises linearly with vanadium addition up to 0.2 atomic ratio, after which there is a further dramatic increase in catalytic activity (Fig. 6). With this jump in activity there is an increase in carbon oxide production and a decrease in the selectivity to acrylonitrile. From FT-IR spectra, one can relate this jump in activity, seen with 0.3 atomic ratio of vanadium, to the presence of V=O groups of the V_2O_5 phase, responsible for deep oxidation products. Two hypotheses are put forward to explain the FT-IR data; that the vanadate stretches at 840 and 990 cm^{-1} are due to (i) an amorphous $SbVO_4$, or (ii) due to vanadium species formed by the incorporation of vanadium atoms within the nickel antimonate tri-rutile structure. In other words a new ternary system has been formed.

From Table 2, the effect of vanadium in modifying the activity of $NiSb_2O_6$, is further demonstrated. The yield to acrylonitrile, in propene ammoxidation, is raised from 18 to 75% under isothermal conditions at 390°C, proving that vanadium is involved not only in the activation of the paraffin but also in the ammoxidation of the olefin. These data indicate that the binary nickel antimonate is very selective to ACN but shows poor activity. With the vanadium-doped nickel antimonate, both the conversion and the selectivity to ACN remain high, resulting in a good yield in the desired product. Besides that, the ternary compound not only is more active and selective than Ni–Sb, but also than V–Sb. These data seem to support the hypothesis that a new ternary phase containing nickel, vanadium, and antimony has been formed, rather than a nickel antimonate with an amorphous layer of $SbVO_4$.

Figure 9 compares the sum of the yields in by-products (acetonitrile and hydrogen cyanide) in propene and

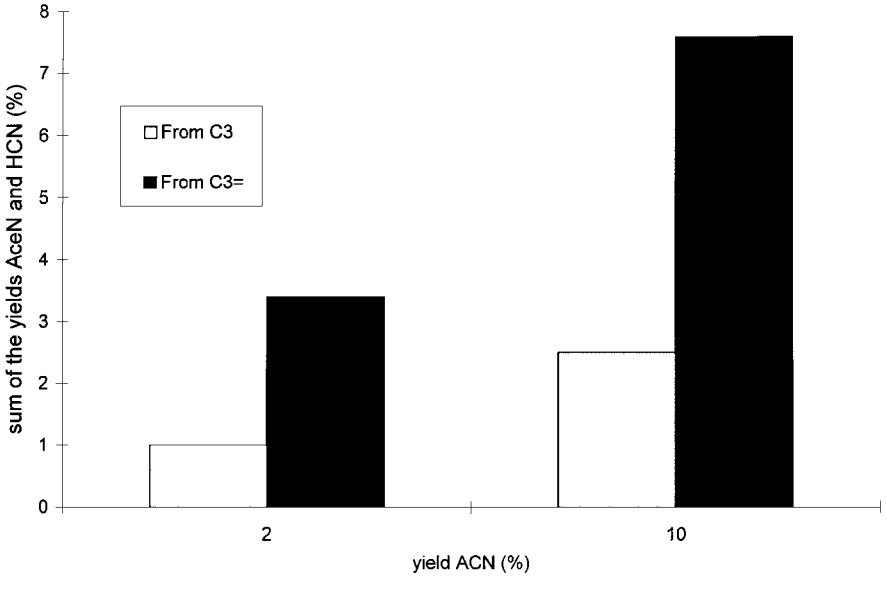

FIG. 9. Comparison of the sum of by-products (AceN and HCN) with equal ACN yields in the ammoxidation of propane and propene over NiSbV 1/2/0.2.

propane ammoxidation at equal yields in acrylonitrile. This figure demonstrates that propane ammoxidation is a much cleaner reaction than propene ammoxidation. The smaller amounts of hydrogen cyanide and acetonitrile formed in propane ammoxidation, notwithstanding the fact that the mechanistic pathway is through propene, may be explained by the low surface concentration of propene. The propene formed in the oxidation of propane is, in fact, very quickly transformed to acrylonitrile over nickel vanadium antimonate catalysts.

The coprecipitation procedure employed and a calcination temperature of 700°C overnight, ensured catalysts with high surface areas and with a high degree of homogeneity. This resulted in an intimate interaction between vanadium, antimony, and nickel and may favour the formation of surface ternary compounds that are active and selective in the ammoxidation of propane.

Furthermore, while propene was always found as a product over Sb–V based systems, with our system very little was detected. This demonstrates the multifunctional properties of the vanadium-doped nickel antimonate catalysts; that is, not only do they activate propane, they also manage to be very active and selective in propene ammoxidation.

ACKNOWLEDGMENTS

T.J.C. is grateful to The Royal Society of Great Britain for providing a European Scholarship. This work was sponsored by M.U.R.S.T. (Ministero dell'Università e della Ricerca Scientifica e Tecnologica).

REFERENCES

1. Centi, G., and Trifirò, F., *Catal. Today* **3**, 151 (1988).
2. Seshan, K., *Appl. Catal.* **67**, N5 (1990).
3. Oshima, K., Kayo, A., Umezawa, T., Kiyono, K., and Sawaki, I., Europ. Patent 529,853 A2, 1992. [Assigned to Mitsubishi Kasei Co.]
4. Kahney, R. H., and McMinn, T. D., U.S. Patent 4,000,178, 1976. [Assigned to the Monsanto Co.]
5. Honda, T., and Terada, K., Europ. Patent 428,413 A1, 1990. [Assigned to Mitsui Toatsu Chem. Inc.]
6. Guttmann, A. T., Grasselli, R. K., and Brazdil, J. F., U.S. Patent 4,746,641 (1988).
7. Bradzil, J. F., Little, I. B., and Hazen, J. B., U.S. Patent 5,214,016 (1993). [Assigned to The Standard Oil Co.]
8. (a) Osipova, Z. G., and Sokolovskii, V. D., *Kinet. & Katal.* **20**, 510,512, (1979); (b) Osipova, Z. G., Sokolovskii, V. D., and Burylin, S. Yu., *Kinet. & Katal.* **24**, 639 (1983); (c) Osipova, Z. G., and Sokolovskii, V. D., *et al., Kinet. & Katal.* **30**, 494, 1251 (1983).
9. (a) Moro-oka, Y., *et al.*, "Catal. Sci. and Technology," Vol. 1, p. 439 (S. Yoshoda, N. Takezawa, and T. Ono, Eds.), Kodansha, Tokyo/VHC, Weinhein, 1990. (b) Moro-oka, Y., "New Developments in Selective Oxidation" (G. Centi and F. Trifirò, Eds.), p. 491, Elsevier, Amsterdam, 1990.
10. (a) Minow, G., Schnabel, K. H., and Öhlmann, G., *React. Kinet. Catal. Lett.* **22**, 399 (1983); (b) Minow, G., and Schnabel, K. H., *Z. Phys. Chem. (Leipzig)* **265**, 145 (1984).
11. Trifirò, F., *Catal. Today* **16**, 91 (1993).
12. Andersson, A., Andersson, S. L. T., Centi, G., Grasselli, R. K., Sanati, M., and Trifirò, F., *in* "New Frontiers in Catalysis" (L. Guczi *et al.*, Eds.), p. 691, Elsevier Science, Amsterdam, 1993.
13. Centi, G., Grasselli, R. K., Patane, E., and Trifirò, F., *in* "New Developments in Selective Oxidation" (G. Centi and F. Trifirò, Eds.), p. 515, Elsevier Science, Amsterdam, 1990.
14. Catani, R., Centi, G., and Trifirò, F., *Indus. Eng. Chem. Rev.* **31**, 107 (1992).
15. Centi, G., Grasselli, R. K., and Trifirò, F., *Catal. Today* **13**, 661 (1992).
16. Cavani, F., and Trifirò, F., *Appl. Catal. A* **88**, 115 (1992).
17. Moro-oka, Y., and Ueda, W., *Catalysis* [R. Soc. Chem.] **223**, 11 (1994).
18. Albonetti, S., Blanchard, G., Burattin, P., Cavani, F., and Trifirò, F., French Patent 94-07982, 1994. [Assigned to Rhone Poulenc Chimie.]
19. Wells, A. F., "Structural Inorganic Chemistry," Clarendon, Oxford, 1962.
20. Sala, F., and Trifirò F., *J. Catal.* **41**, 1 (1976).
21. Berry, F. J., *Adv. Catal.* **30**, 97 (1981).
22. Husson, E., Repelin, Y., and Brusset, H., *Spectrochim. Acta A* **35**, 1177 (1979).
23. Bordoni, S., Castellani, F., Cavani, F., and Trifirò, F., *J. Chem. Soc. Faraday Trans.* **90**(19), 2981 (1994).
24. Juàrez Lòpez, R., Godjayeva, N. S., Cortès Corberàn, V., Fierro, J. L. G., and Mamedov, E. A., *Appl. Catal. A* **124**, 281 (1995).
25. Powder Diffraction File—Inorganic Phases, International. Centre for Diffraction Data, PA, USA (1991).
26. Grasselli, R. K., *in* "Surface Properties and Catalysis by Non-Metals" (J. P. Bonnelle, B. Delmon, and B. Derouane, Eds.), p. 273, Kluwer Academic, Amsterdam, 1982.